Tracer diffusion and thermal stability in amorphous Co-Zr and their relevance for solid-state amorphization

Wolfgang Dörner* and Helmut Mehrer
Institut für Metallforschung, Universität Münster, Wilhelm-Klemm-Strasse 10, D-4400 Münster, Germany
(Received 3 December 1990)

Measurements have been made of tracer diffusion, thermal relaxation, and crystallization in amorphous $Co_{89}Zr_{11}$ samples prepared by melt spinning in vacuum. The diffusivity in as-quenched material is enhanced due to the presence of quasivacancies (excess free volume). During an annealing treatment, the quasivacancies are eliminated and the diffusivity approaches a constant value that depends on temperature only and pertains to a metastable equilibrium state. Tracer self-diffusion of ^{57}Co measured over the temperature range 513–693 K in relaxed amorphous material can be described by

$$D(^{57}\mathrm{Co}) = 8.03\times10^{-7}\exp\left[-\frac{147\ \mathrm{kJ\,mol^{-1}}}{RT}\right]\ \mathrm{m^2\,s^{-1}}\ .$$

Tracer diffusion of ^{195}Au in the temperature range 633–684 K is represented by

$$D(^{195}\mathrm{Au}) = 7.90\times10^{-1}\exp\left[-\frac{274\ \mathrm{kJ\,mol^{-1}}}{RT}\right]\ \mathrm{m^2\,s^{-1}}\ .$$

Co is a fast diffusor as compared to Au, which very likely diffuses at a similar rate as zirconium. Crystallization studies were made by means of differential scanning calorimetry. The diffusion of Co in amorphous Co-Zr can explain quantitatively the growth rates of amorphous interlayers by solid-state amorphization reactions (SSAR's) in the Co-Zr system reported in the literature. Significant atomic motion at temperatures at which SSAR occurs is restricted to Co diffusion, which explains that diffusion limited growth of an amorphous phase can take place without nucleation of the more stable intermetallic compounds. The activation enthalpy of crystallization (335 kJ mol^{-1}) is much higher than the enthalpy of Co diffusion.

I. INTRODUCTION

Amorphous alloys (metallic glasses) are nonequilibrium structures with no long-range crystalline or compositional order. Short-range order is usually present in metallic glasses. Their structure is similar to that of supercooled liquids and approaches a dense random packing of atoms. The densities of amorphous alloys are slightly less than those of comparable crystalline phases.

Amorphous alloys are interesting materials for diffusion studies. From a scientific point of view the atomic mechanism of diffusion in amorphous solids are still poorly understood. From a technological viewpoint a knowledge of the atomic mobility is an important prerequisite for development and applications of metastable materials.

Measurements of diffusivities in metallic glasses are relatively sparse because of the inherent metastability of the amorphous phase. For reviews of the field, see Cantor and Cahn,[1] Limonge, Brebec, and Adda,[2] Cantor,[3] and Mehrer and Dörner.[4] A comprehensive collection of data can be found in Ref. 5. Many of the more stable metallic glasses crystallize rapidly at temperatures between 400 and 600 °C. Diffusivities below the crystallization temperature are usually less or even much less than 10^{-17} $m^2\,s^{-1}$. Such small diffusivities are often measured by Rutherford backscattering spectrometry, secondary-ion mass or Auger spectroscopy, or by fairly indirect techniques like the growth of crystallites during primary crystallization. Only a few direct measurements using radioactive tracers in combination with a sputtering technique for serial sectioning have been carried out.[6–13]

Earlier measurements of diffusion in metallic glasses often scatter so much that they cannot be used to deduce reliable information on the temperature dependence of the diffusivities, let alone to permit conclusions on the atomic mechanisms of diffusion. Furthermore, in some of the earlier investigations it has not been taken into account that the structure of the glass is not fixed like that of a crystalline solid, but can be a function of the quenching rate during glass formation. As a consequence in subsequent thermal treatments an irreversible structural relaxation towards a relaxed metastable amorphous structure can take place. Diffusivities in as-quenched amorphous alloys can be enhanced due to the presence of quenched-in excess free volume (excess quasivacancies) and drop when this is eliminated during irreversible structural relaxation processes.[4,7,9–11,14]

The discovery of Schwarz and Johnson[15] that interdiffusion in thin film multilayers of crystalline metals can lead to amorphization has raised further interesting questions which concern the diffusion-controlled kinetics of this solid-state amorphization reaction (SSAR). In the meantime a series of binary systems, mostly on the basis of one early transition metal (e.g., Ti,Zr,Hf,. . .) and one of the late transition metals (e.g., Fe,Co,Ni,. . .) have been discovered in which the amorphous state is attainable by solid-state interdiffusion. Reviews are given by Johnson,[16,17] Gerl and Guilmin,[18] and by Samwer.[19]

The discovery of Koch *et al.*[20] that mechanical alloying (MA) of crystalline powders of Ni and Nb in a ball mill leads to amorphization appears to be a closely related phenomenon in which interdiffusion in the fine-lamellar microstructure created during ballmilling very likely is the key process of amorphization. In recent years amorphization by mechanical alloying has been reported for numerous binary systems. For reviews see, e.g., Schultz[21,22] and Weeber and Bakker.[23] Very recently in our laboratory it has been demonstrated that the systems Nb-Fe, Nb-Co, Nb-Cr, and Nb-Mn get amorphous during ballmilling.[24]

Among the many systems that are known to undergo SSAR Co-Zr is one of the most thoroughly studied systems due to the work of the Göttingen-Aarhus group.[25–29] However, direct diffusion studies in amorphous Co-Zr have been missing. It is one of the aims of the present study to provide such data.

The amorphous Co-Zr samples used for the present study were produced by melt spinning in vacuum as described in Sec. II. Diffusion studies were performed by the radio-tracer method using ^{57}Co and ^{195}Au and ion-beam sputtering as serial sectioning technique. This technique permits the measurement of atomic motion over a few ten to about 10^3 nm. This is necessary since an initially amorphous sample could not be expected to retain its amorphous structure during diffusion anneals that would lead to atomic motion over such large distances which could be measured by conventional serial sectioning techniques. The noncrystallinity of the samples after typical anneals was checked by x-ray diffraction and transmission electron microscopy.

In the present study we use the ^{195}Au isotope as a substitute for a Zr radioisotope which was not available with sufficient specific activity during the time of the present experiments. Because of its fairly large atomic radius Au should diffuse at a similar rate as Zr.

Diffusion was studied in as-quenched and in preannealed samples. The temperature dependences of the diffusivities were investigated for preannealed samples. This procedure was chosen since only in the relaxed metastable state can reliable information on the temperature dependence be deduced. The data for the relaxed amorphous material are compared to literature data available for amorphous Fe-Zr and Ni-Zr alloys and to data for comparable crystalline phases (Sec. III).

The thermal stability of amorphous Co-Zr was investigated by differential scanning calorimetry (DSC). From the exothermal effects associated with crystallization measured at several heating rates, an activation enthalpy of crystallization was deduced (Sec. IV) which could be compared to the activation enthalpies of diffusion.

The present study provides directly measured diffusion coefficients in amorphous Co-Zr. In Sec. V these data will be compared with interdiffusion coefficients determined from the growth kinetics of the amorphous phase in SSAR experiments. The relevance of the present data for SSAR will be discussed in detail.

II. EXPERIMENTAL PROCEDURE

A. Preparation of amorphous samples

Samples were prepared from cobalt pieces (99.5% purity) and zirconium pieces (99.8% purity) both obtained from Cerac Inc. To remove oxidation and other surface contaminants the Co pieces were etched in a 1:1 mixture of methanol and HNO_3 and the Zr pieces in a mixture of 90 ml H_2O, 90 ml HNO_3, and 5 ml HF. After cleaning and drying the metal slugs the cobalt was degassed by melting it several times in an electron-beam furnace (Leybold-Heraeus Inc.).

Preweighed amounts of Co and Zr were alloyed in the composition $Co_{89}Zr_{11}$ by electron-beam melting under a vacuum better than about 2 mPa. This composition was chosen because it corresponds to the position of a deep eutectic in the Co-Zr phase diagram.[30] The alloy was homogenized by cutting the crystalline bar (about 200 g) into smaller pieces and melting them together in the electron-beam furnace. This procedure was repeated several times. The composition and homogeneity was checked in an electron-beam microprobe (ARL SEMQ 51). For further details the reader is referred to Ref. 31.

Amorphous ribbons were produced with a vacuum melt-spinning rig (Edmund Bühler Inc.) which was modified according to our purpose. The vacuum during the melt-spinning process was typically several mPa. About 20 g of the alloy ingot was placed inside a quartz tube with a 0.04×1 cm slot in one end and was vacuum melted by induction heating. The temperature of the alloy was monitored by a pyrometer (Maurer Inc.). When the temperature had reached about 1300 °C the melt was forced through the slot with purified argon gas of typically 7–9 kPa in a thin stream onto a wheel of 16 cm in diameter rotating at a speed of about 31 m s^{-1}. The wheel had been machined from a *Cu*CrZr alloy (Zollern Stahl und Metall Inc.). Before each run it was polished carefully with fine grid silicon carbide and microsheet paper to a mirror finish and cleaned with acetone to minimize surface contamination.

Ribbons about 40 μm thick and 1 cm wide were obtained. Subsequent x-ray-diffraction studies disclosed no signs of crystallinity. Figure 1 shows an example for an x-ray diffractogram taken in a diffractometer with monochromator using Mo $K\alpha_1$ radiation.

B. Diffusion measurements

Diffusion experiments were performed on round samples with 8–9 mm in diameter punched from the amorphous ribbons. The diffusion surface to be covered with a radiotracer layer was lapped with 1 μm grade Al_2O_3 sus-

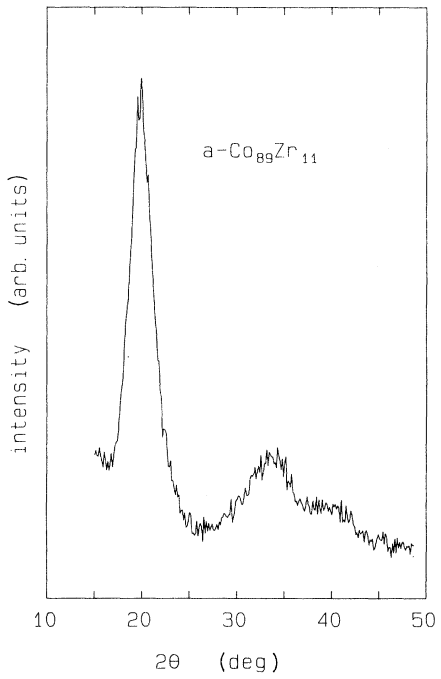

FIG. 1. X-ray diffractogram (Mo $K\alpha_1$ radiation) of an amorphous $Co_{89}Zr_{11}$ ribbon produced by melt spinning.

pension and then polished with colloidal silicic acid (Syton) on a metallurgical cloth. After polishing the samples were carefully cleaned in ultrasonic baths of acetone and ethanol. Samples which were used in structural relaxation studies were immediately deposited with a ^{57}Co tracer film (see below).

Samples used to study the temperature dependence of the diffusivity in the relaxed amorphous state were preannealed before deposition of the tracer. Preannealing treatments were performed at 633 K for 1–6 h. The purpose of this annealing was to establish a metastable equilibrium structure and to avoid significant effects of structural relaxation during the subsequent diffusion anneal.

Deposition of the radiotracers onto the diffusion samples was performed in a vacuum chamber at a pressure of 0.2 mPa. Two different tracer materials were employed. The carrier-free ^{57}Co isotope with a half-life of 271 d was purchased as chloride (NEN Corp.) with a specific activity higher than 150 MBq/μg cobalt. Several μl were dried on a W foil which was then used as an evaporation boat. The isotope ^{195}Au was obtained from the mass 195 of the mercury beam produced by the ISOLDE facility at CERN in Geneva. ^{195}Hg was implanted with 60 keV into a W foil. Within a few hours the ^{195}Hg decays into its long-lived daughter nuclide with a half-life of 183 d which then is absolutely carrier free and radiochemically pure because it has passed a mass seperator. Later on the W foil was used as an evaporation boat. The projected range of the implanted ^{195}Au atoms is only 20–30 nm. The evaporation of the Au atoms from the W foil proved to be quite efficient. The ^{57}Co coated samples were diffused by inserting the sealed quartz ampoule inside a preheated stainless-steel block at the center of a resistance furnace.

The ^{195}Au coated samples were wrapped into cleaned Ta foil and annealed in a UHV system described elsewhere.[32,33] The temperature was measured by a Ni/Cr-Ni thermocouple and continuously recorded. Warming-up and cooling-down corrections were performed when necessary.

C. Concentration profile analysis

The ^{57}Co and ^{195}Au concentration profiles in diffused samples were determined by a sputter-sectioning technique employing a sputtering rig described elsewhere.[34] The specimen was fixed in the center of a Cu specimen holder using a conducting paint and sputtered by high-purity (99.999%) Ar ions with fixed energies between 500 and 1000 eV. The specimen holder was rotated during sputtering for uniformity of the sputtering rate. The current between sample holder and the anode of the ion source was continuously recorded and usually found to be constant. The sputtering rate was corrected for small changes of the current which sometimes occurred.

The total penetration distance was evaluated from the total weight loss during sputtering, the specimen area, and the density of the material which was measured to be 8.20 g cm^{-3} for the amorphous ribbon. Typical weight losses during sputtering of about 100 μg were determined within ± 1 μg using a Sartorius microbalance.

A constant fraction of the material removed by sputtering was collected on a Nalophan foil (Hoechst AG) which was advanced stepwise and subsequently cut into pieces corresponding to each section. The count rate of each section was determined in a well-type NaI(Tl) crystal scintillation detector (^{57}Co diffusion: γ rays at 122 and 136 keV) or a liquid scintillation counter (^{195}Au diffusion: γ rays 98.9 keV) using "Opti-Fluor O" (Packard Instruments Inc.) as scintillation cocktail.

D. Check of noncrystallinity

In order to control whether the samples remained amorphous during the preannealing treatments and the subsequent diffusion anneals all samples were checked by x-ray diffraction analyses after the sputtering process following the diffusion runs. X-ray diffractograms taken on samples after the sectioning procedure are shown in Fig. 2. They disclose no signs of crystallinity.

Reference samples were prepared for transmission electron microscope studies by the electrolytic jet polishing technique with a mixture of CH_3OH and $HClO_4$ (2:1 ratio by volume) at 263 K, 13.5 V, and 200 mA. The samples were analyzed in a Hitachi H-800 NA transmission electron microscope using an acceleration voltage of 200 kV.

Figure 3 shows an electron diffraction image of a sample after a typical preannealing treatment (633 K, 6 h) clearly indicating that the material was still in the amorphous state. Figure 4 shows a micrograph taken after an extended anneal (683 K, 24 h). A small crystallite embedded into an amorphous matrix is visible. However, this

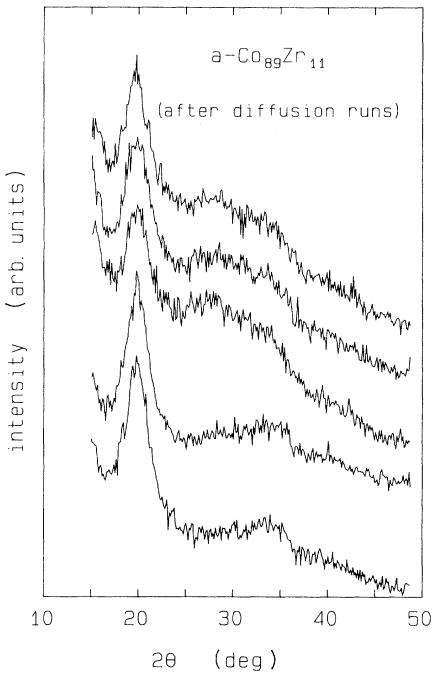

FIG. 2. X-ray diffractograms (Mo $K\alpha_1$ radiation) of $Co_{89}Zr_{11}$ diffusion samples after the diffusion anneals.

picture is not typical in the sense that the total crystallized fraction was estimated to be not more than 1%.

E. DSC measurements

Exothermal effects resulting from crystallization of the amorphous $Co_{89}Zr_{11}$ alloy were measured in a differential scanning calorimeter. A DSC 7 delta (Perkin Elmer Inc.) was used for these measurements. Samples were typically 3–5 mg in weight and were enclosed in Al pans. During the calorimeter runs the Al pans were held inside the calorimeter cell under an atmosphere of Ar, which was renewed at a rate of 20–30 cm^3/min. The calorimeter was calibrated by the melting temperatures of indium and zinc.

The peak temperature, T_x, at which the maximum of the heat flow occurs from a thermally activated transformation like crystallization is a function of the heating rate α at which the sample is heated. The heating rate of the calorimeter was varied between 2 and 100 K min^{-1}. As the heating rate is increased T_x increases as well. The activation enthalpy, Q_x, for the process can be obtained according Kissinger's equation[35]

$$\ln\left[\frac{\alpha}{T_x}\right]=-\frac{Q_x}{RT_x}+\text{const} \tag{1}$$

from the slope of a plot of $\ln(\alpha/T_x)$ versus $1/T_x$.

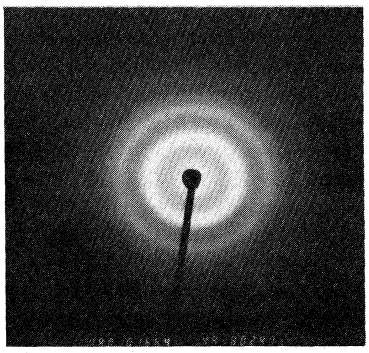

FIG. 3. Electron diffraction pattern of a $Co_{89}Zr_{11}$ sample after a preannealing treatment.

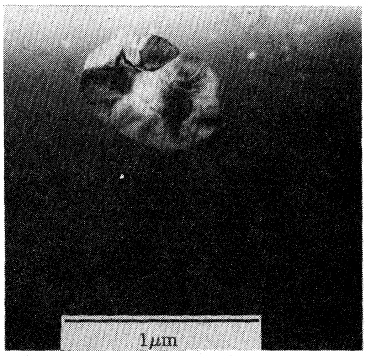

FIG. 4. Electron micrograph showing a small crystallite embedded into the amorphous matrix after a 24-h anneal at 683 K.

III. RESULTS AND DISCUSSION OF DIFFUSION STUDIES

A. Diffusion in as-quenched samples

Concentration-depth profiles from amorphous $Co_{89}Zr_{11}$ samples which were ^{57}Co coated in the as-quenched state are shown in Fig. 5. All samples were diffusion annealed at the same temperature (633 K) for six different times between 24 and 1150 min. Except for the first few sections the plots of logarithm of the specific activity versus penetration distance x squared are straight lines over one to two orders of magnitude indicating that the profiles match a Gaussian concentration distribution

$$c(x,t)=c_0\exp\left[-\frac{x^2}{\sigma_A^2}\right]. \tag{2}$$

σ_A^2 is the variance of the distribution and c_0 a constant. After a long enough diffusion anneal σ_A^2 is dominated by the diffusive broadening.

The deviations for the Gaussian behavior near the surface are probably due to surface hold up; it may be caused by oxidation of near surface layers, which then act as a barrier against diffusion, or by difficulties in dissolving Co. Similar surface hold up was also reported for Co diffusion in amorphous $Ni_{50}Zr_{50}$ (Ref. 12) and for ^{59}Fe diffusion in amorphous $Fe_{40}Ni_{40}B_{20}$ alloys.[7]

In Fig. 6 the penetration profiles of Fig. 5 are displayed as functions of x^2/t, where t is the time of the diffusion anneal. For diffusion broadening caused by a time-independent diffusivity D

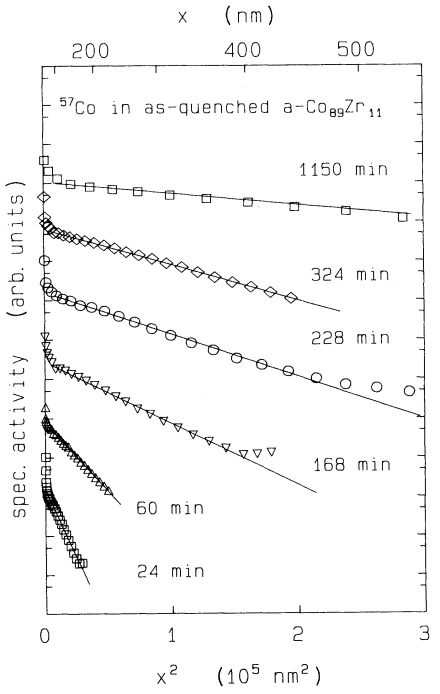

FIG. 5. Concentration-depth profiles of ^{57}Co in as-quenched amorphous $Co_{89}Zr_{11}$ after various diffusion anneals at 633 K.

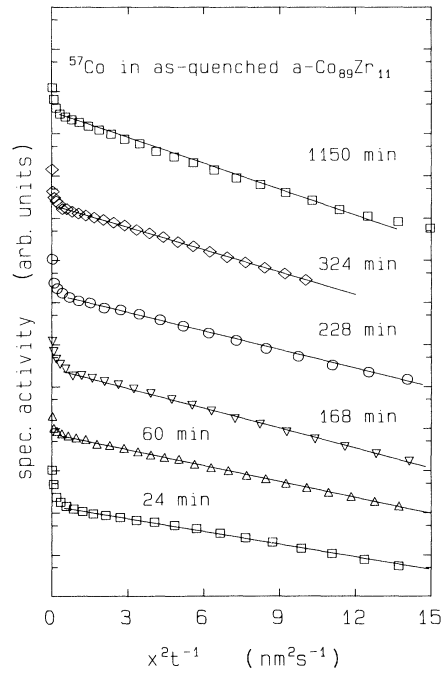

FIG. 6. Concentration-depth profiles of ^{57}Co in as-quenched amorphous $Co_{89}Zr_{11}$ after diffusion anneals at 633 K plotted vs x^2/t.

$$\sigma_A^2 = 4Dt \tag{3}$$

should hold and the slopes in Fig. 5 should be time independent. However, Fig. 6 indicates that the slopes increase with time. This increase could be either due to effects of sputter broadening of the profile or due to a time dependence of the diffusivity due to structural relaxation.

1. *Possible effects of sputter broadening*

The evaluation of diffusion coefficients from very shallow concentration profiles could be complicated by the measurement technique used: a δ function in concentration is broadened to the inherent depth resolution of the sputtering process. This depth resolution is of the order of a few nm. The measured concentration depth profile is then the convolution of the actual concentration with the instrumental broadening.

Diffusion is a further source of Gaussian broadening. The measured concentration in a sample after annealing is given by a Gaussian with variance σ_A^2 which is given by

$$\sigma_A^2 = 4\langle D \rangle t + \sigma_B^2 , \tag{4}$$

where σ_B^2 is the variance of the broadening due to the measuring process such as mixing of atoms due to knock-on effects and surface roughness. $\langle D \rangle$ is the tracer diffusion coefficient observable in as-quenched samples during a diffusion anneal of duration t. The broadening due to diffusion alone is given by the difference $\sigma_A^2 - \sigma_B^2$. If the instrumental broadening and the concentration depth profile after the diffusion anneal both fit Gaussians, values of σ_B and σ_A could be determined directly. Often the depth resolution σ_B is not measured in a separate experiment.

In the present experiments σ_B was determined to be of the order of 4–6 nm. To get further insight we rewrite Eq. (4) in the following way:

$$\frac{\sigma_A^2}{4t} = \langle D \rangle + \frac{\sigma_B^2}{4t} . \tag{5}$$

The quantities $\sigma_A^2/4t$ have been deduced from the linear portions of the penetration curves of Fig. 5 and are plotted in Fig. 7 as a function of $1/t$. The dashed line in Fig. 5 corresponds to a typical value of instrumental broadening ($\sigma_B = 6$ nm). Figure 7 clearly indicates that the decrease of $\sigma_A^2/4t$ with increasing time cannot be attributed to the depth resolution of the sputter process but is mostly due to a decrease of $\langle D \rangle$ with increasing time. Such a decrease should be expected if irreversible structural relaxation of the as-quenched amorphous sample occurs during the diffusion anneal.

2. *Diffusivity enhancement in the unrelaxed state*

The preceding discussion has shown that the observed decrease in diffusivity in as-quenched amorphous Co-Zr is indeed mainly an effect of structural relaxation of the materials towards a metastable equilibrium state. The

values of the diffusivity measured on as-quenched samples are then to be identified with the time-averaged diffusivity

$$\langle D \rangle = \frac{1}{t} \int_0^t D(t')dt' , \tag{6}$$

where D denotes the instantaneous diffusivity.

Values of $\langle D \rangle$ determined from the profiles of Fig. 5 are plotted in Fig. 8. From Fig. 8 values for the instantaneous diffusivity have been deduced using the relationship

$$D(t) = \frac{d(\langle D \rangle t)}{dt} = \langle D \rangle + t\frac{d\langle D \rangle}{dt} . \tag{7}$$

The values of $D(t)$ are displayed in Fig. 8 as a dashed line. After several hours at 633 K the diffusivity reaches a plateau regime where $\langle D \rangle$ and D are (almost) time independent. These values can be attributed to the amorphous alloy in its metastable equilibrium state.

Similar effects of diffusivity enhancement in the unrelaxed state have been observed by Horvath and Mehrer[7] for amorphous $Fe_{40}Ni_{40}B_{20}$ and by Horvath *et al.*[11] for a whole series of amorphous Fe base alloys. Irreversible structural relaxation of amorphous alloys leads from a less stable to a more stable—but still metastable—amorphous state. During irreversible structural relaxation quenched-in excess free volume (excess quasivacancies) is eliminated by the thermal treatment. As discussed already in Ref. 7 and later on in more detail by Frank, Horvath, and Kronmüller[14] the diffusivity enhancement in unrelaxed amorphous alloys represents contributions of tracer diffusion via excess quasivacancies. A remainder of free volume left over after irreversible structural relaxations, however, is inherent to the relaxed amorphous state. Without this minimum of free volume the material would crystallize.

B. Diffusion in preannealed samples

In this section we consider diffusion results for preannealed amorphous $Co_{89}Zr_{11}$. The purpose of the preannealing treatment (see Sec. II) was to remove quenched-in quasivacancies and to bring the samples close to metastable equilibrium prior to the diffusion experiments.

Penetration profiles of ^{57}Co and ^{195}Au diffusion profiles from preannealed (^{57}Co: 633 K, 1 h; ^{195}Au: 633 K, 6 h) amorphous samples are displayed in Figs. 9 and 10, respectively. The diffusion data are listed in Tables I and II. The D values have been deduced from the fits of the thin-film solution of Fick's second law to the linear portions of the plots of Figs. 9 and 10. Displayed in the Arrhenius diagram of Fig. 11 are the temperature dependences of ^{57}Co and ^{195}Au diffusivities. Within the experimental accuracy they exhibit an Arrhenius-type behavior. Least-squares fits of the diffusion data yield

$$D(^{57}Co) = 8.03 \times 10^{-7} \exp\left[-\frac{147 \text{ kJ mol}^{-1}}{RT} \right] \text{m}^2\text{s}^{-1} \tag{8}$$

and

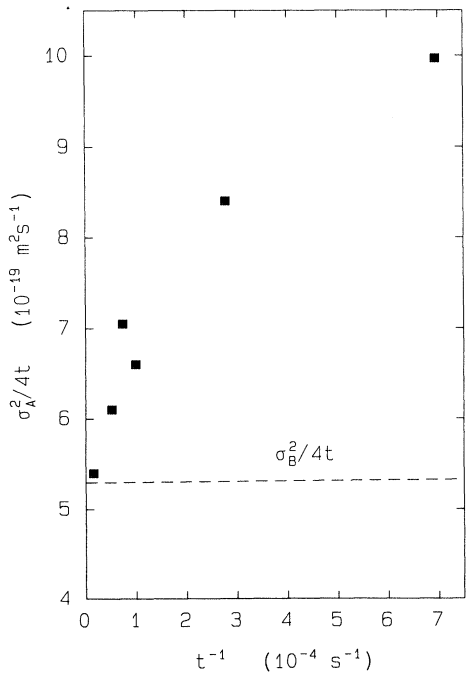

FIG. 7. Plot of $\sigma_A^2/4t$ vs $1/t$ for as-quenched $Co_{89}Zr_{11}$ at 633 K. The instrumental broadening $\sigma_B^2/4t$ is indicated as a dashed line for $\sigma_B = 6$ nm.

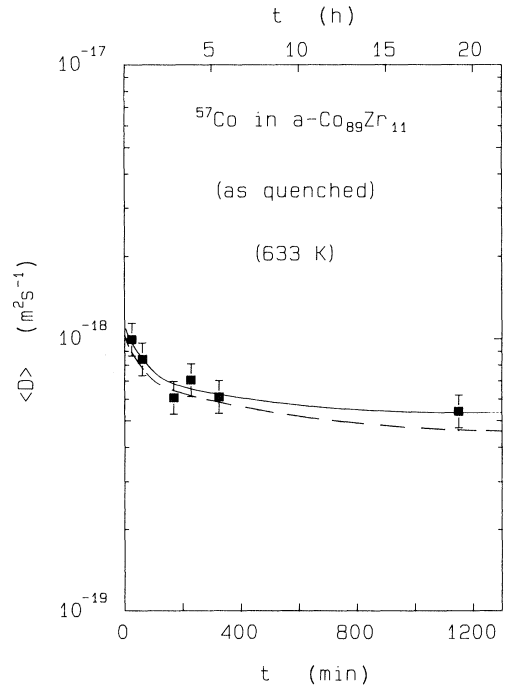

FIG. 8. Effect of structural relaxation on the diffusivity of ^{57}Co in as-quenched amorphous $Co_{89}Zr_{11}$. The annealing temperature is 633 K.

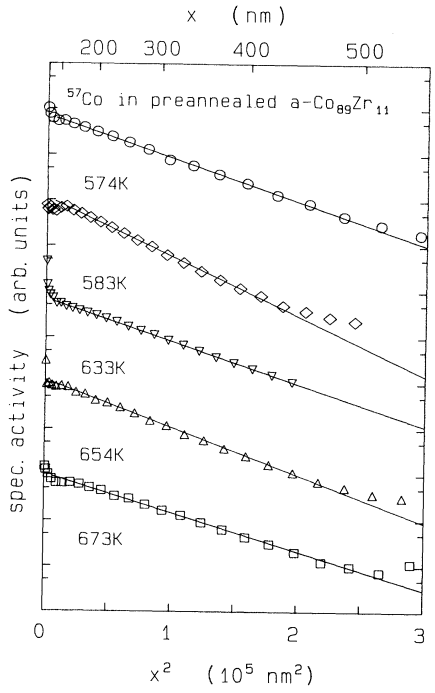

FIG. 9. Concentration-depth profiles of ^{57}Co in preannealed amorphous $Co_{89}Zr_{11}$ for various temperatures.

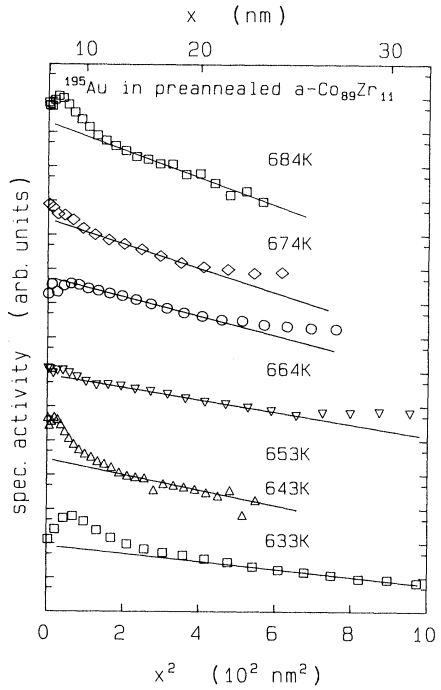

FIG. 10. Concentration-depth profiles of ^{195}Au in preannealed amorphous $Co_{89}Zr_{11}$ for various temperatures.

$$D(^{195}\mathrm{Au}) = 7.90\times10^{-1}\exp\left[-\frac{274\ \mathrm{kJ\,mol^{-1}}}{RT}\right]\ \mathrm{m^2\,s^{-1}}\ . \tag{9}$$

The ^{195}Au data have been corrected for the effect of instrumental broadening using $\sigma_B = 5.3$ nm. In the case of ^{57}Co diffusion this correction was unnecessary because of the larger diffusion depths.

1. *Comparison with previous diffusion measurements in late transition-metal zirconium glasses*

For amorphous Co-Zr there are no tracer diffusion data available in the literature. In Fig. 12 the values of diffusion coefficients determined in the present experiments are compared with those of other zirconium containing glasses with Ni or Fe as the second constituent: Horvath *et al.*[11] have investigated ^{59}Fe and ^{95}Zr diffusion in melt-spun Fe-Zr alloys. The [Fe]/[Zr] ratio in their $Fe_{91}Zr_9$ alloy is very similar to the [Co]/[Zr] ratio in the present $Co_{89}Zr_{11}$ alloy. Also shown are the data of Hahn and Averback[36] and Hoshino *et al.*[13] who have studied the diffusion of ^{63}Ni, ^{60}Co, Cu, and Au atoms in coevaporated amorphous $Ni_{50}Zr_{50}$. Stelter and Lazarus[37] have made measurements of Ag and Au foreign atom diffusion in melt-spun amorphous $Cu_{50}Zr_{50}$ samples using Auger-electron spectrometry for Ag and Rutherford backscattering spectrometry for Au. Because Cu is not a late transition metal these data are not included in Fig. 12.

Some important features of Fig. 12 may be noted in the following:

(1) Co in $Co_{89}Zr_{11}$, Fe in $Fe_{91}Zr_9$, and Ni in $Ni_{50}Zr_{50}$ diffuse at very similar rates.

TABLE I. Diffusion data for ^{57}Co diffusion in preannealed amorphous $Co_{89}Zr_{11}$.

T (K)	t (min)	D (m^2 s^{-1})	$2\sqrt{Dt}$ (nm)
693	60	7.16×10^{-18}	321
682	60	4.53×10^{-18}	255
673	60	3.46×10^{-18}	223
654	120	1.46×10^{-18}	205
633	228	7.05×10^{-19}	196
633	168	6.59×10^{-19}	163
633	324	6.10×10^{-19}	218
613	390	3.30×10^{-19}	176
602	360	1.75×10^{-19}	123
583	2430	5.68×10^{-20}	182
574	6720	2.86×10^{-20}	215
552	18682	6.99×10^{-21}	177
533	28640	3.03×10^{-21}	144
513	87840	1.49×10^{-21}	177

TABLE II. Diffusion data for ^{195}Au diffusion in preannealed amorphous $Co_{89}Zr_{11}$.

T (K)	t (min)	σ_A^2 (nm^2)	$\sigma_A^2-\sigma_B^2$ (nm^2)	D (m^2 s^{-1})	$2\sqrt{Dt}$ (nm)
684	1440	362.9	334.9	9.69×10^{-22}	18.3
674	1620	192.5	164.5	4.23×10^{-22}	13.9
664	4320	239.5	211.5	2.04×10^{-22}	14.5
653	5770	153.7	125.7	9.08×10^{-23}	11.2
643	8640	121.3	93.3	4.50×10^{-23}	9.7
633	18660	110.6	82.6	1.84×10^{-23}	9.1

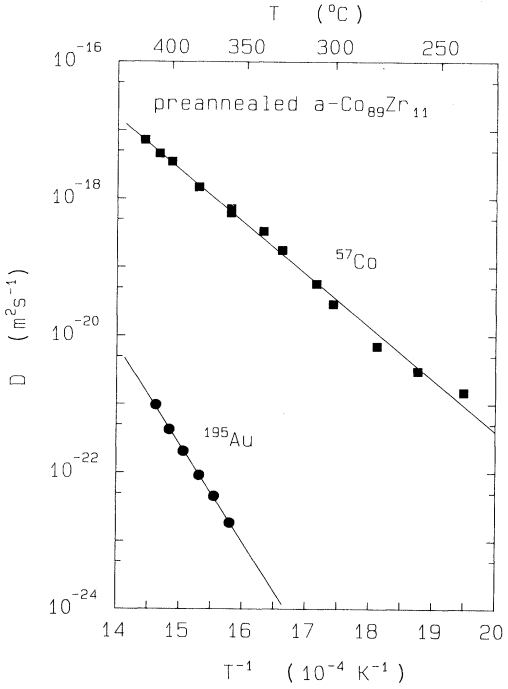

FIG. 11. Arrhenius diagram of Co and Au diffusion in preannealed amorphous $Co_{89}Zr_{11}$.

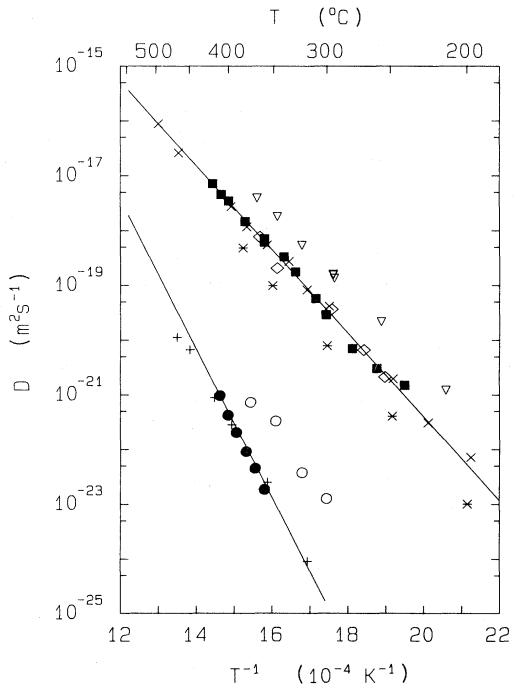

FIG. 12. Comparison between the Co and Au diffusion in amorphous $Co_{89}Zr_{11}$ and various literature data on binary Zr containing amorphous alloys: ■, ^{57}Co in a-$Co_{89}Zr_{11}$ (this work); ●, ^{195}Au in a-$Co_{89}Zr_{11}$ (this work); ×, ^{59}Fe in a-$Fe_{91}Zr_9$ (Ref. 11); +, ^{95}Zr in a-$Fe_{91}Zr_9$ (Ref. 11); △, ^{60}Co in a-$Ni_{50}Zr_{50}$ (Ref. 12); ◇, ^{63}Ni in a-$Ni_{50}Zr_{50}$ (Ref. 12); ⁎, Cu in a-$Ni_{50}Zr_{50}$ (Ref. 36); △, Au in a-$Ni_{50}Zr_{50}$ (Ref. 36).

(2) Au in $Co_{89}Zr_{11}$, Au in $Ni_{50}Zr_{50}$, and Zr in $Fe_{91}Zr_9$ diffuse at similar rates.

(3) The late transition element constituents of the alloys (Co in $Co_{89}Zr_{11}$, Fe in $Fe_{91}Zr_9$, Ni in $Ni_{50}Zr_{50}$) are relatively *fast* diffusors.

(4) The striking similarities between the diffusion rates of the late transition element constituents and the proximity of Au diffusion rates in $Co_{89}Zr_{11}$ and $Ni_{50}Zr_{50}$ to those of Zr self-diffusion in $Fe_{91}Zr_9$ permit the following hypothesis: Zr atoms are *slow* diffusors in amorphous Co-Zr and Ni-Zr alloys as well.

2. *Comparison with diffusion in α-zirconium and cobalt*

A comparison of the present diffusion results for amorphous Co-Zr with diffusion in crystalline Co and α-Zr is shown in Fig. 13. Diffusivities in the amorphous alloy are higher than self-diffusion in both elements[38,39] but considerably lower than Co diffusion data in α-Zr.[40,41]

It is well known that Co like the other late transition elements (Fe, Ni, . . .) is an extremely rapid diffusor as compared to self-diffusion of Zr atoms in α-Zr. The atomic radius of Co (0.125 nm) is considerably smaller than that of Zr (0.159 nm). For crystalline zirconium Hood[42] has pointed out an empirical relation between the diffusivity and the atomic radius of the diffusing atom.

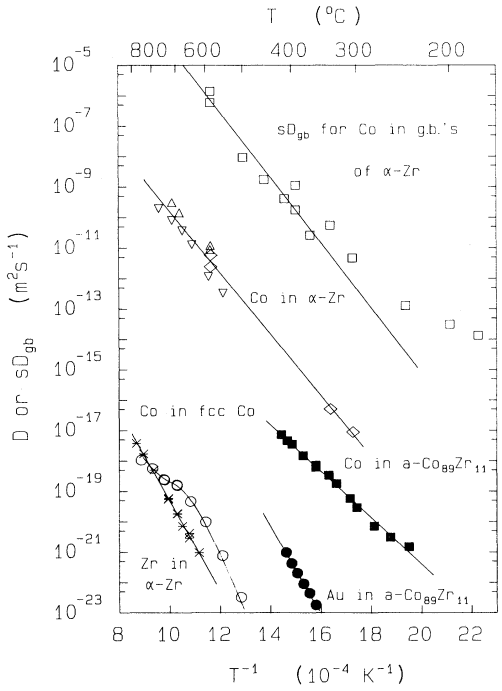

FIG. 13. Comparison between the present Co- and Au-diffusion data in amorphous $Co_{89}Zr_{11}$ and various diffusion phenomena in α-zirconium and cobalt: ■, Co in a-$Co_{89}Zr_{11}$ (this work); ●, Au in a-$Co_{89}Zr_{11}$ (this work); △, ▽, Co in α-Zr parallel and perpendicular to the c axis (Ref. 40); ◇, Co in α-Zr polycrystals (Ref. 41); ○, Zr self-diffusion in α-Zr (Ref. 39); ⁎, Co self-diffusion in fcc Co (Ref. 38); □, sD_{GB} for Co diffusion in grain boundaries of α-Zr (s = segregation factor) (Refs. 41 and 43).

The diffusivity increases drastically with decreasing atomic radius. The high diffusivities of the small late transition atoms in crystalline Zr are commonly attributed to an interstitial diffusion mechanism whereas Zr self-diffusion occurs via a vacancy mechanism.

A similar correlation between the atomic radii was found by Hahn and Averback[36] for diffusion of various atoms in amorphous $Ni_{50}Zr_{50}$. The present results show a similar correlation (see Fig. 12) for amorphous $Co_{89}Zr_{11}$. Co atoms with small atomic radius diffuse orders of magnitude faster than the larger Au atoms (0.142 nm) in amorphous Co-Zr.

The diffusion of Co along grain boundaries of α-Zr is by far the fastest diffusion process indicated in Fig. 12. The values of sD_{GB} (s = segregation factor, D_{GB} = grain boundary diffusivity) were obtained from the data of Vieregge and Herzig[43] (see also Ref. 41) using a value of 5×10^{-10} m for the grain boundary width. Since the segregation factor can hardly exceed 10^3-10^4 (Ref. 43), the grain boundary diffusivity is still several orders of magnitude higher than Co diffusion in the amorphous alloy.

3. *Diffusion mechanisms in amorphous late transition metal-zirconium alloys*

A consistent interpretation of the results is possible if we assume that the relaxed amorphous structure is basically stable and that the diffusion rates are governed by the jump distances and the local environment of the diffusing atom, which is not very dissimilar to those for a crystalline solid.

Like in crystalline α-Zr *small atoms* in amorphous alloys between late transition metals (LTM's) and zirconium appear to diffuse by an *interstitial-like mechanism,* using interstices of the amorphous structure as jump positions. Small values of the preexponential factors and of the activation enthalpies are well-known features of interstitial diffusors in crystalline solids. Table III shows that late transition-metal atoms are indeed diffusors with relatively small preexponential factors and activation enthalpies.

The diffusion mechanism of *large atoms,* however, is very likely different from a simple monovacancy mechanism with thermal vacancies which is well known to govern self-diffusion in crystalline metals. Table III shows that the preexponential factors for diffusion of large atoms are larger than those of self-diffusion of close-packed crystalline Co and Ni and even much larger than those of the small atoms in the amorphous alloys. Nevertheless, the diffusivity of large atoms like Zr and Au is considerably faster than self-diffusion in any of the crystalline late transition metals or in α-Zr (see Fig. 13).

For $Fe_{91}Zr_9$ it has been observed that in the relaxed amorphous state a temperature change from T_1 to T_2 gives rise to a delay-free change in the diffusivity. Using this observation Kronmüller and Frank[44] try to rule out quasivacancies present in thermal equilibrium as diffusion vehicles and argue in favor of a direct diffusion mechanism. On the other hand in SSAR experiments (see Sec. V for details) on Co-Zr systems pores have been observed at the position of the original Co layers and have been interpreted as Kirkendall voids.[26] It is well-known that Kirkendall voids in crystalline substitutional alloy diffusion couples are a strong indication that vacancies are involved as diffusion vehicles which may agglomerate into voids on the side of the faster diffusing species of the couple (see e.g., Ref. 45). Therefore, either the interpretation of the observed pores in terms of Kirkendall voids or the hypothesis of a direct diffusion mechanism needs further consideration.

In any case the migration of large atoms in an amorphous structure in contrast to smaller atoms requires the collective displacement of a group of surrounding atoms. Since in such a mechanism many atoms move collectively larger diffusion entropies and hence fairly high preexponential factors become understandable.

IV. RESULTS OF CRYSTALLIZATION STUDIES

The heat evolved from amorphous $Co_{89}Zr_{11}$ on heating a small piece of the material in the DSC at a constant rate of 50 K min^{-1} is displayed in Fig. 14. The exothermic peak arises from the crystallization of the sample. (Occasionally two nearly crystallization peaks have been observed for $Co_{89}Zr_{11}$.[31] In such a case the position of the main peak corresponds to the peak shown in Fig. 14.)

The crystallization enthalpy, ΔH_x, which is the enthalpy difference between the amorphous and the crystalline

TABLE III. Activation enthalpies and preexponential factors for diffusion in amorphous zirconium containing alloys and fcc cobalt and nickel.

Matrix	Diffusor	D^o (m^2 s^{-1})	Q (kJ mol^{-1})	Reference
a-$Co_{89}Zr_{11}$	^{57}Co	8.03×10^{-7}	147	This work
	^{195}Au	7.90×10^{-1}	274	
a-$Ni_{50}Zr_{50}$	^{63}Ni	1.70×10^{-7}	140	12
	^{60}Co	3.70×10^{-7}	135	
a-$Fe_{91}Zr_9$	^{59}Fe	3.10×10^{-7}	145	11
	^{95}Zr	2.10×10^{-3}	241	
fcc Co	^{57}Co,^{58}Co,^{60}Co	5.50×10^{-5}	289	38
fcc Ni	^{63}Ni	1.33×10^{-4}	281	57

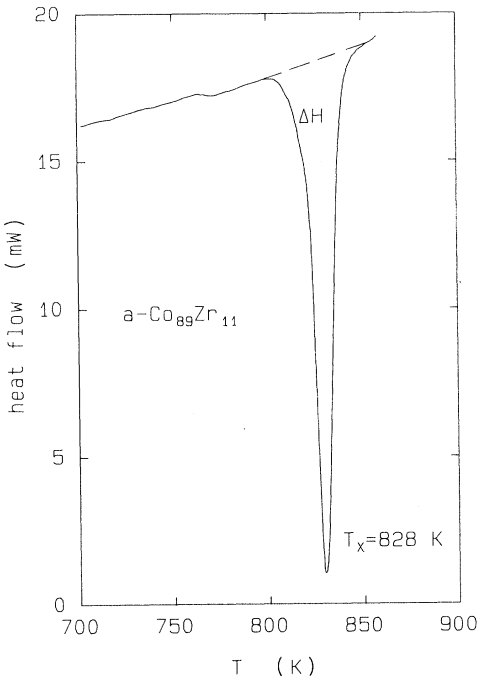

FIG. 14. DSC thermogram of the crystallization of amorphous $Co_{89}Zr_{11}$ at a heating rate of 50 K min^{-1}.

phase(s), can be deduced from the area between the DSC trace and the baseline. We obtain a value of

$$\Delta H_x = 3.8 \pm 0.2 \text{ kJ mol}^{-1} .$$

Table IV shows the crystallization temperatures T_x (peak temperature) and the onset temperatures T_o for the various heating rates. The peak temperature data are displayed in the Kissinger plot of Fig. 15. From the slopes we get for the activation enthalpy of crystallization

$$Q_x = 335 \text{ kJ mol}^{-1} .$$

We estimate an uncertainty in the activation enthalpy of about 5%.

V. TRACER DIFFUSION IN AMORPHOUS Co-Zr AND SOLID-STATE AMORPHIZATION

It has been often stated in the literature without direct experimental proof that solid-state amorphization by interdiffusion (SSAR) (see, e.g., Johnson,[46] Samwer,[47] and Cahn[48]) is entirely dependent on the rapid diffusion of one of the two atomic species through the amorphous layer combined with very slow diffusion of the other component.

Before we compare diffusion data from our tracer studies with those determined from the SSAR experiments we review some important features of SSAR on Co-Zr or closely related systems: Multilayer samples of crystalline Co and Zr layers 20–100 nm thick are prepared by sequential evaporation of the two elements onto a substrate. The thin-film multilayer sample is then annealed at temperatures between 200 and 250 °C. The temperature has to be sufficiently high to promote appreciable diffusion. However, the formation of crystalline intermetallic CoZr compounds at higher temperatures imposes an upper limit for the temperatures of an SSAR experiment.

TABLE IV. Peak and onset temperatures for the crystallization of a-$Co_{89}Zr_{11}$ for various heating rates.

α (K min^{-1})	T_x (K)	T_o (K)
2	776.8	774.9
5	784.9	782.4
7	790.3	787.3
10	795.2	788.9
13	799.7	795.5
20	810.0	805.3
30	812.7	807.4
50	823.4	815.6
70	827.1	819.1
100	833.2	823.9

The *nucleation process* of the amorphous phase has attracted considerable attention. The experiments show that the amorphization starts at every interface between the crystalline Co or Ni and Zr layers. Zirconium grain boundaries and/or triple points of zirconium grain boundaries and the Co/Zr interface seem to be important as nucleation sites for SSAR. Vredenberg *et al.*[49] used single-crystalline zirconium and a polycrystalline Ni and observed no amorphization after thermal treatment. In a complementary experiment Pampus, Samwer, and Bottiger[50] used single-crystalline Ni evaporated onto a poly-

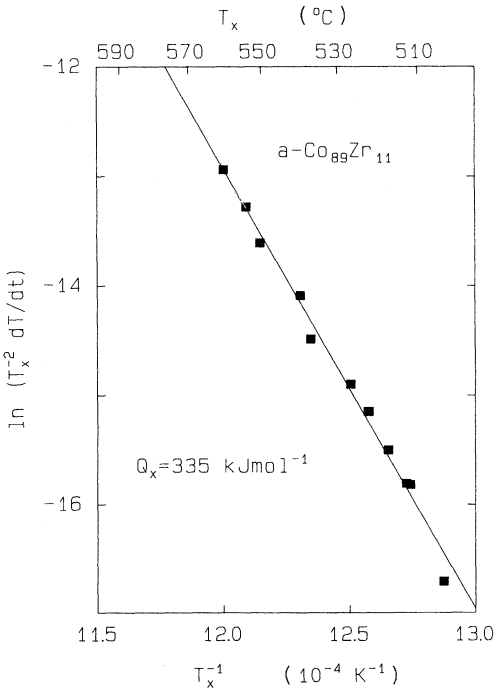

FIG. 15. Kissinger-Boswell plot of the crystallization peak temperatures, T_x, and the corresponding heating rate α.

crystalline Zr layer. No nucleation barrier was present in this case. Recently, based on experiments of Co diffusion along grain boundaries of polycrystalline α-Zr Vieregge and Herzig[43] (see also Ref. 41) have proposed a model of the nucleation of the amorphous phase at triple points between Zr grain boundaries and the Co/Zr interface.

In contrast to the nucleation process, which so far has not been observed directly, the *growth kinetics* of the amorphous phase has been studied in Co-Zr layer systems by several authors and was found to be entirely diffusion controlled. The amorphous phase grows as a *uniform, planar* interlayer between the crystalline Co and Zr layers. This geometry is clearly revealed by cross-sectional transmission electron micrographs taken during an intermediate state of the SSAR reaction. The *thickness* of the amorphous interlayers as a function of annealing time has been studied using Rutherford-backscattering spectrometry (RBS), cross-section transmission electron microscopy (CS-TEM), x-ray diffraction (XRD), and electrical resistivity measurements on bilayer and multilayer samples. For long times the thickness of the amorphous layer increases with the square root of time indicating diffusion-controlled growth. Interdiffusion coefficients derived from the parabolic growth law are listed in Table V together with the method used and the references.

A comparison between the present tracer diffusion data in amorphous Co-Zr and the interdiffusion coefficients listed in Table V is displayed in Fig. 16. In view of the uncertainties involved in this comparison which, e.g., concern the unknown thermodynamic factor in the interdiffusion coefficient and the fact that the SSAR experiments were performed on diffusion couples with somewhat higher Zr content, the D values are in fairly good agreement.

This leads to the important conclusion that (at least for larger reaction times) the relatively fast Co diffusion in the amorphous alloy is indeed the time-limiting process of SSAR. During an SSAR experiment Co diffuses through the amorphous interlayer and reacts with crystalline Zr at the interface between the amorphous alloy and Zr.

TABLE V. Diffusion coefficients determined in various SSAR experiments on Co-Zr.

T (K)	D ($m^2 s^{-1}$)	Method	Reference
554	3.4×10^{-20}	RBS	25
534	9.7×10^{-21}		
523	7.3×10^{-21}		
513	2.3×10^{-21}		
522	1.0×10^{-20}	Resistivity	26
497	3.6×10^{-21}	(bilayers)	
473	7.8×10^{-22}		
522	1.1×10^{-20}	Resistivity	26
497	2.3×10^{-21}	(multilayers)	
473	1.0×10^{-21}		
523	1.0×10^{-20}	CS-TEM	26
523	1.0×10^{-21}	XRD	27

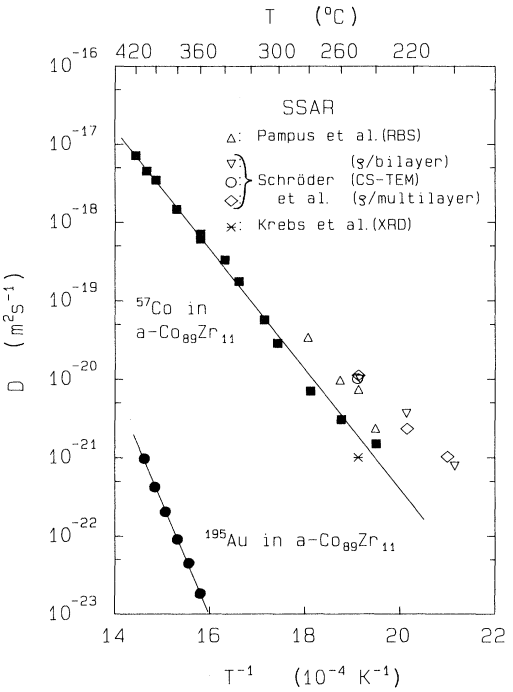

FIG. 16. Comparison between the present Co- and Au-tracer diffusion data in amorphous $Co_{89}Zr_{11}$ and interdiffusion coefficients determined from the growth kinetics of amorphous layers in SSAR experiments (see also Table V).

So far we have not discussed the question, why the crystalline intermetallic Co-Zr compound(s) which correspond to the thermodynamic equilibrium state are not formed during a SSAR experiment. Following Johnson[16,17] thermodynamic requirements of SSAR are illustrated in Fig. 17. G_o, G_x, and G_a denote the Gibbs free energies of the initial state (crystalline elemental multilayer sample), of the stable intermetallic phase(s), and of the metastable amorphous phase, respectively.

A diagram of the Gibbs free energies versus concentration for the Co-Zr system representing the intermetallic stochiometric compounds, the fcc Co and hcp Zr solid solutions, and the amorphous phase was deduced by Gärtner and Bormann[51] using Calphad calculations.

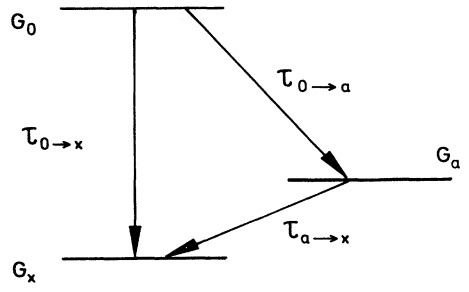

FIG. 17. Schematic illustration of the transition from a high-energetic initial state to the thermodynamic equilibrium state and to the metastable state.

Large values of the order of 30–40 kJ mol^{-1} for G_o-G_a are reported. By contrast the enthalpies of crystallization for amorphous Co-Zr are much lower. Values between 2.3 and 6.1 kJ mol^{-1} have been determined in our DSC measurements (see Sec. IV and Ref. 31) depending on the composition of the amorphous samples (3.8 kJ mol^{-1} for a-$Co_{89}Zr_{11}$). It is obvious that the heat of mixing—the driving force to form an alloy—is large as compared to the crystallization enthalpy—the energy associated with crystalline order. As a consequence the small difference in the Gibbs free energies G_x and G_a results in similar driving forces for the nucleation of the intermetallics and of the amorphous phase.

The formation of the metastable amorphous phase can be understood from a kinetic point of view. According to Johnson[17] SSAR can be expected if the time scale for amorphization is characterized by a time constant ($\tau_{o\to a}$) which is small as compared to the time constants of nucleation and growth of the equilibrium intermetallics ($\tau_{o\to x}$) and the time constant for the crystallization of the amorphous phase ($\tau_{a\to x}$):

$$\tau_{o\to a} \ll \tau_{o\to x}, \tau_{a\to x} \ . \tag{10}$$

The differences in time constants must be attributed to the nucleation and growth processes of the various phase transitions.

It has been argued by several authors[18,52] that the interface energy between the amorphous phase and the crystalline phase(s) analogous to the interface energy between a melt and the pertaining crystalline phase is small as compared to (the) interphase energie(s) between the intermetallic equilibrium compound(s) and the crystalline elements. This favors the formation of an amorphous phase already during the nucleation regime.

The time constant for the growth of an amorphous layer of thickness d in an SSAR experiment is of the order of

$$\tau_{o\to a} \approx \frac{d^2}{D} \ . \tag{11}$$

In other words, the time constant $\tau_{o\to a}$ is small because Co is a rapid diffusor in amorphous Co-Zr.

The *crystallization* of an amorphous alloy occurs via nucleation and growth of the crystalline phase(s) similar to the crystallization of an undercooled liquid. The theory of nucleation of crystals in undercooled metals was developed by Turnbull[53] and others.[54] Nucleation phenomena can be investigated indirectly by analyzing the microstructure of an amorphous alloy after some amount of crystallization and by extrapolating growth reactions to shorter times.[55] Once a stable nucleus is formed, it will continue to grow with a velocity which is thermally activated. Techniques such as DSC provide data on reaction kinetics and activation enthalpies for larger transformed fractions. This regime of the crystallization is dominated by the growth kinetics. Thus the activation enthalpy for growth should be the same as the overall activation enthalpy for crystallization.

Various micromechanisms of crystal growth can be distinguished in amorphous alloys (see, e.g., Ref. 55). The interpretation of the activation enthalpy of crystallization in a given amorphous alloy depends on the actual micromechanism.

Linear growth is observed for *eutectic and polymorphic crystallization.* A stable nucleus will grow with a velocity

$$u = u_o \exp\left[-\frac{Q_g}{RT}\right] , \tag{12}$$

where Q_g is the activation enthalpy for growth. u_0 is a characteristic velocity given by the product of the Debye frequency times the distance across the crystallization front (about 0.5 nm). Parabolic growth is observed for *primary crystallization.* A particle of radius r grows with a velocity given by

$$u = \tfrac{1}{2}\beta^2 \frac{D}{r} \ , \tag{13}$$

where β is a dimensionless parameter which can be evaluated from the composition at the particle interface and the composition of the sample. Contrary to eutectic or polymorphic crystallization the activation enthalpy of this crystallization mode is an activation enthalpy of diffusion.

The micromechanism of crystallization of amorphous $Co_{89}Zr_{11}$ was studied by Altounian, Shank, and Strom-Olsen.[56] Primary crystallization seems to be the dominating crystallization mode. This is in agreement with x-ray studies of Sprengel, Dörner, and Mehrer[31] performed on crystallized $Co_{89}Zr_{11}$, in which ϵ-Co was identified as a crystallization product.

The activation enthalpy of crystallization for $Co_{89}Zr_{11}$ determined from a Kissinger analysis of the DSC experiments in Sec. IV was $Q_x = 335$ kJ mol^{-1}. Our experiments of tracer diffusion have revealed a large difference in the diffusivities and activation enthalpies of Co and Zr atoms in amorphous Co-Zr. We have argued that the activation enthalpy, Q_{Zr}, for Zr diffusion is close to the value, Q_{Au}, for Au diffusion:

$$Q_{Zr} \simeq Q_{Au} = 274 \text{ kJ mol}^{-1} \ .$$

Clearly the activation enthalpy for Co diffusion is much lower than Q_x. On the other hand, the values for the activation enthalpies for crystallization of $Co_{89}Zr_{11}$ and for diffusion of Zr atoms are then not very dissimilar indicating that a certain atomic mobility of Zr is indispensible for the crystallization of the amorphous Co-Zr.

VI. SUMMARY AND CONCLUSIONS

Tracer diffusion studies were performed on as-quenched and preannealed amorphous $Co_{89}Zr_{11}$ produced by melt spinning:

(1) The diffusivity of ^{57}Co was determined in as-quenched material as a function of the diffusion time. A diffusivity enhancement with respect to preannealed material is observed. It is attributed to an excess of quasivacancies (free volume) which anneals out when the material approaches its metastable equilibrium state.

(2) The temperature dependences for the diffusivities of ^{57}Co and ^{195}Au in preannealed material are described by Arrhenius equations. The activation parameters for Co

diffusion (8.03×10^{-7} $m^2 s^{-1}$, 147 kJ mol^{-1}) are considerably lower than those for Au diffusion (7.90×10^{-1} $m^{-2} s^{-1}$, 274 kJ mol^{-1}). Au very likely diffuses at a similar rate as Zr atoms.

(3) Similar to the fast diffusion of Co in crystalline zirconium Co is a fairly rapid diffusor in the amorphous alloy as well. The difference between the rapid diffusion of late transition metals and the sluggish self-diffusion is, however, less pronounced in amorphous alloys than in crystalline zirconium.

(4) Small atoms like Co diffuse by a direct interstitial-like mechanism, using the interstices of the amorphous structure as jump positions.

(5) In contrast to smaller atoms the migration of larger atoms like Au and Zr requires the collective displacement of several surrounding atoms leading to higher values for the diffusion enthalpies and entropies.

The crystallization behavior was studied by differential scanning calorimetry:

(6) The activation enthalpy of crystallization (335 kJ mol^{-1}) is much higher than the diffusion enthalpy of Co and only slightly higher than the diffusion enthalpy of Au in the amorphous material.

With respect to relevance of the diffusion and crystallization studies for the solid-state amorphization reaction (SSAR) we come to the following conclusions:

(7) The diffusivity of Co in amorphous Co-Zr can explain quantitatively the growth rates of amorphous interlayers in SSAR experiments.

(8) Atomic diffusion at temperatures of SSAR experiments in Co-Zr systems is restricted to Co diffusion. The diffusivity of Au and hence of Zr is lower by several orders of magnitude.

(9) Significant diffusion of the Zr constituent will probably result in crystallization of amorphous Co-Zr.

ACKNOWLEDGMENTS

The authors gratefully acknowledge the help of W. Sprengel with the DSC measurements and the help of K. Trinckauf and Professor E. Nembach with TEM work. We also appreciate comments on the manuscript by Dr. N. A. Stolwijk, Professor Ch. Herzig, and G. Rummel. This work was supported by the Deutsche Forschungsgemeinschaft (DFG Me 480/14).

*Present address: Linde AG, D8023 Höllriegelskreuth, Germany.

[1]B. Cantor and R. W. Cahn, in *Amorphous Metallic Alloys,* edited by F. E. Luborski (Butterworths Monographs in Materials, London, 1983), p. 487.

[2]Y. Limonge, G. Brebec, and Y. Adda, in *DIMETA 82—Diffusion in Metals and Alloys,* edited by F. J. Kedves and D. L. Beke, Diffusion and Defect Monograph Ser. 7 (Trans Tech Publications, Aedermannsdorf, 1983), p. 285.

[3]B. Cantor, in *Proceedings of the 5th International Conference on Rapidly Quenched Metals (RQ5),* edited by S. Steeb and H. Warlimont (North-Holland, Amsterdam, 1985), p. 595.

[4]H. Mehrer and W. Dörner, in DIMETA 88—Diffusion in Metals and Alloys [Diffus. Def. Data A **66-69**, 189 (1989)].

[5]J. Horvath, in *Diffusion in Solid Metals and Alloys,* Vol. 26 of *Landolt-Börnstein, New Series, Group III,* edited by H. Mehrer (Springer-Verlag, Berlin 1990).

[6]D. Gupta, K. N. Tu, and K. W. Asai, Phys. Rev. Lett. **35**, 796 (1975).

[7]J. Horvath and H. Mehrer, Cryst. Latt. Def. Amorph. Mater. **13**, 1 (1986).

[8]J. Horvath, K. Freitag, and H. Mehrer, Cryst. Latt. Def. Amorph. Mater. **13**, 15 (1986).

[9]J. Horvath, K. Pfahler, W. Ulfert, W. Frank, and H. Mehrer, J. Phys. (Paris) Colloq. **12**, C8-645 (1985).

[10]J. Horvath, K. Pfahler, W. Ulfert, W. Frank, and H. Kronmüller, Mater. Sci. Forum **15-18**, 523 (1987).

[11]J. Horvath, J. Ott, K. Pfahler, and W. Ulfert, Mater. Sci. Eng. **97**, 409 (1988).

[12]K. Hoshino, R. S. Averback, H. Hahn, and S. J. Rothman, J. Mater. Res. **3**, 55 (1988).

[13]K. Hoshino, R. S. Averback, H. Hahn, and S. J. Rothman, Def. Diffus. Forum **59**, 225 (1988).

[14]W. Frank, J. Horvath, and H. Kronmüller, Mater. Sci. Eng. **97**, 415 (1988).

[15]R. B. Schwarz and W. L. Johnson, Phys. Rev. Lett. **51**, 415 (1983).

[16]W. L. Johnson, Prog. Mater. Sci. **30**, 81 (1986).

[17]W. L. Johnson, Mater. Sci. Eng. **97**, 1 (1988).

[18]M. Gerl, and P. Guilmin, Solid State Phenom. **3+4**, 215 (1988).

[19]K. Samwer, Phys. Rep. **161**, 1 (1988).

[20]C. C. Koch, O. B. Cavin, C. G. Mc Kamey, and J. O. Scarbrough, Appl. Phys. Lett. **43**, 1017 (1983).

[21]L. Schultz, Mater. Sci. Eng. **97**, 15 (1988).

[22]L. Schultz, Phys. Blätter **44**, 247 (1988).

[23]A. W. Weeber and H. Bakker, Physica B **153**, 93 (1988).

[24]M. Schänzer and H. Mehrer, in *Colloque de Physique,* edited by A. R. Yavari and P. J. Desre (Les Editions de Physique, Paris, 1990), p. C4-87.

[25]K. Pampus, J. Bottiger, B. Torp, H. Schröder, and K. Samwer, Phys. Rev. B **35**, 7010 (1987).

[26]H. Schröder, K. Samwer, and U. Köster, Phys. Rev. Lett. **54**, 197 (1985).

[27]H. U. Krebs, and K. Samwer, Europhys. Lett. **2**, 141 (1986).

[28]H. Schröder and K. Samwer, J. Mater. Res. **3**, 461 (1988).

[29]K. Samwer, H. Schröder, and K. Pampus, Mater. Sci. Eng. **97**, 63 (1988).

[30]*Binary Alloys Phase Diagrams,* edited by Th. B. Massalski (American Society for Metals, Metals Park, Ohio, 1986).

[31]W. Sprengel, W. Dörner, and H. Mehrer, Z. Metallk. **18**, 467 (1990).

[32]H. Eckseler and Ch. Herzig, Z. Metallk. **70**, 215 (1979).

[33]K. Vieregge and Ch. Herzig, J. Nucl. Mater. **165**, 65 (1989).

[34]M. Lübbehusen and H. Mehrer, Acta Metall. Mater. **38**, 283 (1990).

[35]H. E. Kissinger, Anal. Chem. **29**, 1702 (1957).
[36]H. Hahn and R. S. Averback, Phys. Rev. B **37**, 6533 (1988).
[37]E. C. Stelter and D. Lazarus, Phys. Rev. B **36**, 9545 (1987).
[38]W. Bussmann, Ch. Herzig, W. Rempp, K. Maier, and H. Mehrer, Phys. Status Solidi A **56**, 87 (1979).
[39]J. Horvath, F. Dyment, and H. Mehrer, J. Nucl. Mater **126**, 206 (1984).
[40]G. V. Kidson and G. J. Young, Philos. Mag. **20**, 1047 (1969).
[41]K. Vieregge, Ph.D. thesis, Universität Münster (1990).
[42]G. M. Hood, J. Nucl. Mater. **159**, 149 (1988).
[43]K. Vieregge and Ch. Herzig J. Nucl. Mater. **175**, 29 (1990).
[44]H. Kronmüller and W. Frank, Radiat. Eff. Def. Solids **108**, 81 (1989).
[45]H. Mehrer, in *Diffusion in Solid Metals and Alloys* (Ref. 5), Chap. 1.
[46]W. L. Johnson, (unpublished).
[47]K. Samwer, Phys. Rep. **161**, 1 (1988).
[48]R. W. Cahn, in *Colloque de Physique* (Ref. 24), p. C4-3.
[49]A. M. Vredenberg, J. F. M. Westendrop, F. W. Saris, N. M. van der Pers, and Th. H. de Keijsar, J. Mater. Res. **1**, 774 (1986).
[50]K. Pampus, K. Samwer, and J. Bottiger, Europhys. Lett. **3**, 581 (1987).
[51]F. Gärtner and R. Bormann, in *Colloque de Physique* (Ref. 24), p. C4-95.
[52]R. W. Cahn and W.L. Johnson, J. Mater. Res. **1**, 724 (1986).
[53]D. Turnbull, Contemp. Phys. **10**, 473 (1960).
[54]H. Biloni, in *Physical Metallurgy,* edited by R. W. Cahn and P. Haasen (North-Holland, Amsterdam, 1983).
[55]U. Köster, Z. Metallk. **75**, 691 (1984).
[56]Z. Altounian, R. J. Shank, and J. O. Strom-Olsen, J. Appl. Phys. **58**, 1052 (1984).
[57]K. Maier, H. Mehrer, E. Lessmann, and W. Schüle, Phys. Status Solidi B **78**, 689 (1976).

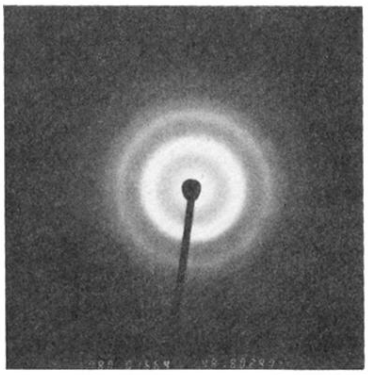

FIG. 3. Electron diffraction pattern of a $Co_{89}Zr_{11}$ sample after a preannealing treatment.

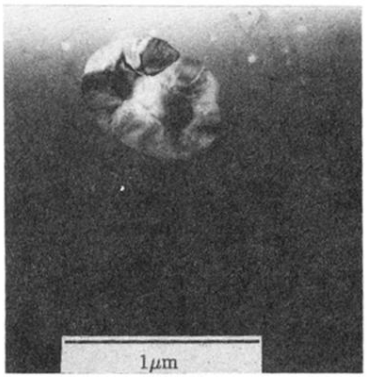

FIG. 4. Electron micrograph showing a small crystallite embedded into the amorphous matrix after a 24-h anneal at 683 K.